

A photometric study of two contact binaries: CRTS J025408.1+265957 and CRTS J012111.1+272933

Shuo Ma^{1,2}, Jin-Zhong Liu^{1,2}, Yu Zhang^{1,2}, Qing-Shun Hu^{1,2}, Guo-Liang Lü³

¹ Xinjiang Astronomical Observatory, Chinese Academy of Sciences, Urumqi, Xinjiang 830011, People's Republic of China; liujinzh@xao.ac.cn

² University of Chinese Academy of Sciences, Beijing 100049, People's Republic of China

³ School of Physical Science and Technology, Xinjiang University, Urumqi, 830064, People's Republic of China

Received 20XX Month Day; accepted 20XX Month Day

Abstract We performed new photometric observations for two contact binaries (i.e., CRTS J025408.1+265957 and CRTS J012111.1+272933), which were observed by the 1.0-m telescope at Xingjiang Astronomical Observatory. From our light curves and several survey data, we derived several sets of photometric solutions. We found that CRTS J025408.1+265957 and CRTS J012111.1+272933 were A- and W-type W UMa, respectively. The results imply that the spot migrates or disappears in two contact binaries, which were identified by chromospheric activity emissions (e.g. H α emission) from LAMOST spectra. From the O-C curves, the orbital periods of two contact binaries may be increasing, which is interpreted by the mass transfer from the less massive component to the more massive one. With mass transferring, two contact binaries may evolve from the contact configurations to semi-detected ones as predicted by the theory of thermal relaxation oscillation.

Key words: binaries: eclipsing – binaries: spectroscopic – stars: distances – stars: fundamental parameters – stars: individual (J0254 and J0121)

1 INTRODUCTION

Eclipsing binaries are some of the most attractive research subjects in stellar astrophysics because they play a significant role in stellar evolution and are currently the most powerful tool to measure stellar parameters. Eclipsing binaries with light variations where there is little difference between primary and secondary eclipsing depths are referred to as W UMa systems. W UMa systems have approximately similar temperatures in both of their components due to a common envelope (Yildiz & Doğan 2013). Normally there is contact between the two components, along with a synchronous circular orbit (Malkov et al. 2006).

W UMa systems, whose spectral classes range generally from F to K, include two late-type dwarf stars that usually exhibit stellar magnetic activities, such as starspots (Kjurkchieva et al. 2019), flares (Huang et al. 2020), chromosphere activity (Whelan et al. 2021) and magnetic activity cycles (Hu et al. 2020). The orbital periods in W UMa systems are usually short, about 0.4 days. It is noteworthy that their orbital periods are generally variational, which

can be attributed to a number of factors, including the mass transfer between the two components (Hoffman et al. 2006), magnetic braking effects (Applegate 1992; Lanza et al. 1998), magnetic cycles (Borkovits et al. 2005), and the third body (Eggleton 2006; Ma et al. 2018). W UMa systems were divided into A- and W-types by Binnendijk (1970) - the hotter component has more mass in A-type systems, while W-type systems are the opposite.

The photometric data of W UMa binaries have recently been released by many surveys, such as the Wide Angle Search for Planets (SuperWASP, Street et al. 2003; Butters et al. 2010), the Catalina Sky Survey (CRTS Drake et al. 2009, 2014), the All-Sky Automated Survey for Supernovae (ASAS-SN, Jayasinghe et al. 2018, 2019, 2020; Pawlak et al. 2019), the Zwicky Transient Facility (ZTF, Bellm et al. 2019), and the Transiting Exoplanet Survey Satellite (TESS, Ricker et al. 2014, 2015). These surveys provide an opportunity for the study of W UMa binaries.

In this paper, we select two W UMa binaries named CRTS J025408.1+265957 (TIC 436926796, 2MASS 02540811+2659578, LPSEB19)(hereinafter as

J0254) and CRTS J012111.1+272933 (TIC 16996819, 2MASS 01211118+2729334, LPSEB31)(hereinafter as J0121) from the catalog of spectral eclipsing binaries (Yang et al. 2020) to investigate their relevant properties. J0254 and J0121 were periodic variable stars (Drake et al. 2014) and were defined as typical W UMa binaries (Jayasinghe et al. 2019). J0254, with an orbital period of 0.311886 days from the International Variable Star Index (VSX¹) or an orbital period of 0.3118858 days (Jayasinghe et al. 2019), is 14.85 or 15.19 mag in V-band mean magnitude, with amplitude of 0.71 or 0.82. Similarly, for J0121, its orbital period is 0.322818 days in VSX² or 0.322819 days in ASAS-SN, with V-band mean magnitude of 14.92 mag and amplitude of 0.53 in VSX, or a V-band mean magnitude of 15.19 mag and amplitude of 0.57 in ASAS-SN.

In our work, we study the parameters, orbital period variation and magnetic activities of the two W UMa binary targets. The paper is organized as follows. In Section 3, we describe the information from the observations and data. The orbital periods are studied in section 3. The chromospheric activity is researched in section 4. The analysis of the light curve is in Section 5. In section 6, we discuss the properties of the two targets. Finally, a summary is shown in Section 7.

2 OBSERVATION AND DATA

2.1 New Observation and Data Reduction

J0254 and J0121 were observed in 2020 with the Nanshan One-meter Wide-field Telescope (Bai et al. 2020, hereafter NOWT) at the Nanshan station of the Xinjiang Astronomical Observatory, which is equipped with a standard Johnson multi-color filter system (e.g., *UBVRI*). A CCD camera, with the pixels of 4096×4136 , 78 arcmin \times 78 arcmin true field, and 1.125 arcsec each pixel scale, is mounted on this telescope.

The Johnson-Cousins *BVRI* filters were used during our observations, with the medium scan rate mode. The observation details, such as the target name, observation date, exposure time, number of images, and mean error of photometric observation, are listed in Table 1. For J0254, a total of 492 CCD images are obtained, and another target (J0121) with 1428 CCD images. The observation precision in more than 90% is better than 0.008 mag. We note that the third observation night of J0121 is slightly less accurate than the other nights (see row 5 of the Mean Error column in Table 1), which is probably due to the weather. The observed CCD images are reduced by the standard

aperture photometry package of the Image Reduction and Analysis Facility (IRAF³) in the standard manner. The process includes image trimming, bias subtraction, flat correction, and aperture photometry. The differential photometry method is adopted in our work. The basic information about the variable stars, the comparison stars, and the check stars are compiled in Table 2, and the partial photometric data are displayed in Table 3.

2.2 Survey Data

The photometric data of J0254 and J0121 are also obtained from the SuperWASP, CRTS, ASAS-SN, and ZTF survey databases. These data are characterized as follows: (a) unfiltered observation and only V-band data available in CRTS; (b) only V-band data in ASAS-SN; (c) ZTF including *g*, *r* bands for our targets; (d) the data in SuperWASP obtained by multiple times scan in same night. There are big magnitude errors in the SuperWASP data for the two targets, which may be because the two targets are outside the suitable magnitude range of the telescope. Among these data, only the SuperWASP data needs to be processed. Therefore, the raw data of SuperWASP were processed in the following steps: firstly, removing the data with magnitude errors greater than 1 mag, then the remaining data with magnitude errors outside three standard deviations being excluded.

In addition, the photometric data of the two objects are also found in TESS database. J0254 was observed in Sectors 18, 42, 43, and 44, while J0121 in Sector 17. The principal data products collected by the TESS mission exist in three forms (the Full Frame Images (FFIs), the Target Pixel Files (TPFs), and the Light Curve Files (LCFs)). Only FFIs, with a cadence of 30 minutes (Sectors 17, 18) and 10 minutes (Sectors 42, 43, 44), of both targets were available. We adopted the python package Lightkurve⁴ to reduce them and obtain the light curves for the two targets by using the PLDCorrector⁵. The TESS data are shown in the upper panel of Fig. 1.

In this paper, we aim to seek the times of minima (eclipse timings) based on the data from TESS, which was used for (*O-C*) analysis. The different methods were used to deal with the data with different cadence. The data with the 30 minutes cadence were clipped and stacked with a similar method adopted by Li et al. (2021) to obtain more times of minima.

For each observation sector, the data of 30 minutes cadence are divided into four parts among which each

¹ <https://www.aavso.org/vsx/index.php?view=detail.top&oid=364624>

² <https://www.aavso.org/vsx/index.php?view=detail.top&oid=362110>

³ <http://iraf.noao.edu/>

⁴ <http://docs.lightkurve.org/>

⁵ <https://docs.lightkurve.org/tutorials/2-creating-light-curves/2-3-k2-pldcorrector.html>

Table 1 Photometric observation log of J0254 and J0121.

Target	UT Date (yyyy-mm-dd)	Exposures(B V R I) (s)	Number(B V R I)	Mean Error(B V R I) (mmag)
J0254	2020-11-06	140 120 100 130	50 49 50 49	8.5 5.9 5.1 6.6
	2020-12-22	96 65 50 60	73 73 74 74	8.2 5.9 5.3 6.5
J0121	2020-09-16	60 40 35 30	83 83 84 84	5.2 4.6 4.4 6.6
	2020-09-17	60 40 35 30	108 109 109 108	5.7 5.1 4.8 6.9
	2020-09-21	60 40 35 30	52 53 53 53	6.7 5.9 5.3 8.1
	2020-09-20	60 40 35 30	112 112 112 113	5.8 5.0 4.5 6.9

Table 2 The coordinates, JHK magnitude of the target stars, comparison stars, and check stars.

Targets	Name	α_{2000}	β_{2000}	Mag_J	Mag_H	Mag_K
Variable star	J0254	02 54 08.11	+26 59 57.9	13.404	13.013	12.887
The comparison	2MASS 02542302+2659315	02 54 22.97	+26 59 31.7	12.306	11.989	11.883
The Check	2MASS 02541421+2705339	02 54 14.16	+27 05 34.5	13.633	13.151	13.016
Variable star	J0121	01 21 11.18	+27 29 33.5	13.667	13.34	13.272
The comparison	2MASS 01211247+2731080	01 21 12.40	+27 31 08.1	13.343	12.982	12.934
The Check	2MASS 01211812+2730019	01 21 18.09	+27 30 02.1	12.766	12.188	12.047

Notes: The coordinates and magnitudes of the variable star and the names, coordinates, and magnitudes of the comparison and check stars are determined from Two Micron All Sky Survey (2MASS; Cutri et al. 2003).

Table 3 Observational data of the two eclipsing binaries obtained in 2020.

Name	Date	HJD. <i>B</i> (2459000+)	$\Delta Mag_{.B}$	HJD. <i>V</i> (2459000+)	$\Delta Mag_{.V}$	HJD. <i>R</i> (2459000+)	$\Delta Mag_{.R}$	HJD. <i>I</i> (2459000+)	$\Delta Mag_{.I}$
J0254	2020-11-06	160.05716497	1.967	160.05893583	1.950	160.06250069	1.953	160.06075295	1.881
	
	2020-12-22	160.45461035	1.342	160.45674003	1.293	160.46029327	1.258	160.45855715	1.217
		205.99502343	1.293	205.99463507	1.263	205.99708356	1.243	205.99730709	1.191
	
		206.32797906	1.374	206.33021230	1.352	206.33109725	1.324	206.33215840	1.280
J0121	2020-09-16	109.18889038	0.180	109.19001316	0.213	109.19086388	0.231	109.19177254	0.238
	
	2020-09-17	109.45586049	0.393	109.45667236	0.432	109.45733632	0.393	109.45808291	0.404
		110.11540897	0.325	110.11592983	0.347	110.11676898	0.368	110.12093008	0.316
	
	2020-09-19	110.45853000	0.193	110.46237136	0.227	110.46303688	0.235	110.46378347	0.253
		112.22555024	0.206	112.22637205	0.246	112.22702601	0.251	112.22777259	0.262
	
		112.40663539	0.170	112.40744563	0.213	112.40811115	0.218	112.40885768	0.223
		114.10625343	0.739	114.11026978	0.717	114.10790283	0.738	114.10864935	0.725
2020-09-21	114.45770486	0.423	114.46191803	0.391	114.46258361	0.378	114.46331851	0.369	

Notes: This table is available in its entirety in machine-readable form.

part was converted into one period through the equation $BJD = BJD_0 + P \times E$, with BJD representing the observing time, BJD_0 denoting the reference time, E referring to the cycle, and the orbital period indicated as P . In this equation, the orbital periods of J0254 and J0121 we adopted were 0.311886 and 0.322818 days in VSX, respectively. By the method, the corresponding four diagrams of J0121 are obtained, as shown in the middle panel of Fig. 1. We can also obtain times of minima on the data of 10 minutes cadence, which based on the manner, that is, the data for each sector is divided into five parts from which the light curve in one period was extracted each part. For example, we displayed the five light curves of J0254 from sector 44 in the bottom panel of Fig. 1.

Except photometric data, the spectral data of the two targets can be found in LAMOST Data Release 7⁶, with five low-resolution spectra for J0254 and two low-

resolution spectra for J0121. Their spectral parameters are tabulated in Table 4, which including the object, observational date, Heliocentric Julian date, phase, spectral type, as well as effective temperature, surface gravity, radial velocity, and their corresponding errors. The phase is calculated based on the linear ephemeris (see more details in Section 3).

3 ORBITAL PERIOD STUDY

In this paper, the higher temperature components of the binary systems were regarded as the primary components. With our observations, the eclipse timings were obtained through the K-W method given by Kwee & van Woerden (1956) from the $BVRI$ -bands light curves. The new times of minima by us and their mean values are shown in Table 5.

In order to study the orbital period variations, we searched for as many eclipse timings of J0254 and J0121

⁶ <http://www.lamost.org/dr7/>

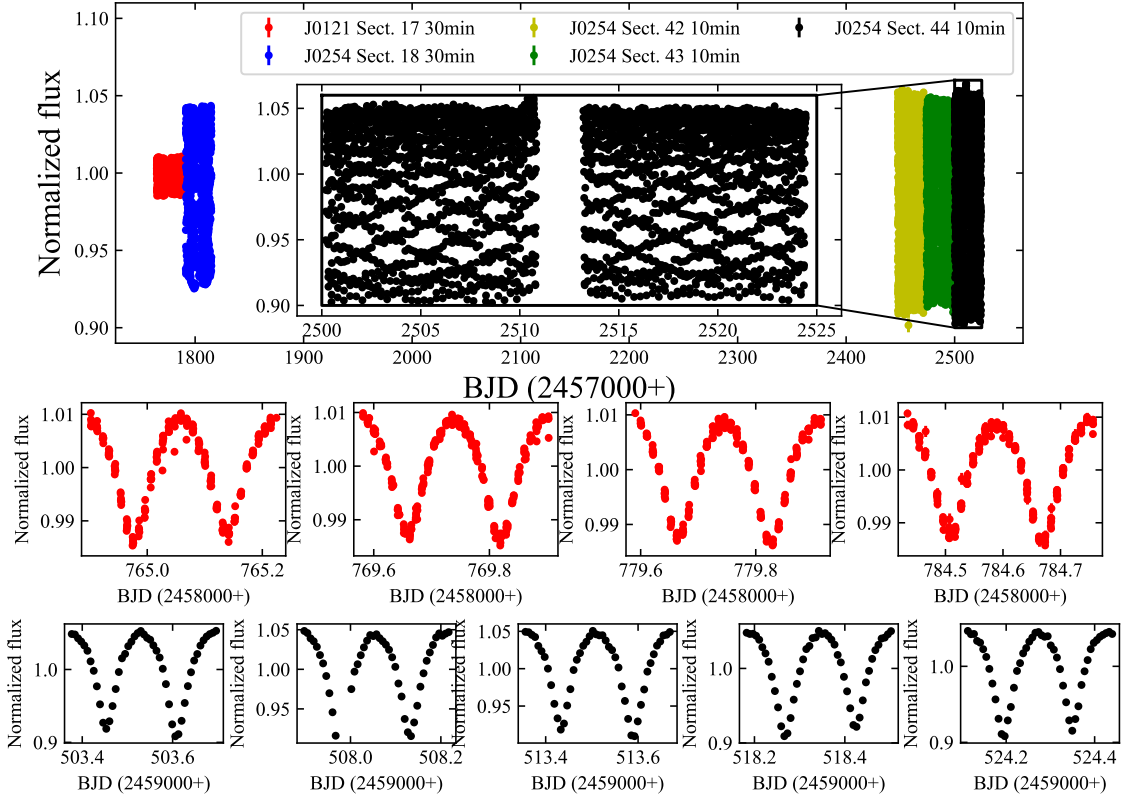


Fig. 1 The upper panel shows the TESS data of J0254 (Sectors 18, 42, 43, 44) and J0121 (Sector 17) and the partial enlargement of the data from sector 44. Then, the J0121 data of 30 minutes cadence are divided into four parts, and the data of each part are transformed into one period and displayed in the middle panel. The data of J0254 from sector 44 are divided into five parts and extracted one period of data from each part and shown in the bottom panel.

Table 4 LAMOST spectral information of J0254 and J0121.

Target	UT Date (yyyy-mm-dd)	HJD (2450000+)	phase	Subclass	T_{eff} (K)	$\log g$	[Fe/H]	Radial velocity ($\text{km}\cdot\text{s}^{-1}$)
J0254	2011-12-03	5899.15799	0.05738	G3				
	2011-12-11	5907.08052	0.45941	F9				
	2012-01-12	5939.01222	0.84208	G3	5594 ± 126	4.24 ± 0.21	-0.20 ± 0.12	-3.2 ± 27.0
	2013-01-16	6308.96913	0.03540	G4	5474 ± 172	4.11 ± 0.27	-0.22 ± 0.16	8.6 ± 12.9
	2013-01-17	6309.97329	0.25504	G7	5565 ± 146	4.18 ± 0.24	-0.07 ± 0.14	-13.0 ± 26.2
J0121	2014-11-11	9278.76899	0.58364	G3	5662 ± 43	4.09 ± 0.07	-0.18 ± 0.04	-37.9 ± 16.3
	2014-12-17	7008.98636	0.42706	G3	5656 ± 27	4.04 ± 0.05	-0.26 ± 0.03	-37.4 ± 10.0

as we could. Thirty-six eclipse timings of J0254 and thirty-two eclipse timings of J0121 were obtained from the SuperWASP database by the K-W method in Nelson’s program⁷. The eclipse timings of J0254 and J0121 can also be found from Yang et al. (2020), who pointed out that these times are primary eclipse timings. In the subsequent analysis, the times of minima were transformed from MJD to HJD through the website⁸. In addition, the times of minima of J0254 and J0121 were also provided by the ASAS-

SN. There are not corresponding errors in the eclipsing times obtained from Yang et al. (2020) and ASAS-SN. Therefore, we set arbitrarily their errors to 0.002 in the following analysis. By the K-W method, we also obtain the eclipse timings based on the light curves in one period from TESS data above. These eclipse timings are transformed from BJD to HJD through the website^{9,10}. In brief, we acquired all times of minima between 2004 and 2021, which were displayed in Table 6.

⁷ <https://www.variablestarsouth.org/software-by-bob-nelson/>

⁸ <http://www.physics.sfasu.edu/astro/javascript/hjd.html>

⁹ <https://astroutils.astronomy.osu.edu/time/bjd2utc.html>, (Eastman et al. 2010)

¹⁰ <http://www.physics.sfasu.edu/astro/javascript/hjd.html>

Table 5 Newly obtained eclipse timings of J0254 and J0121 in the *BVRI* Bands.

	HJD(B)	HJD(V)	HJD(R)	HJD(I)	HJD(average)	Min.
	2459000+	2459000+	2459000+	2459000+	2459000+	
J0254	160.06470±0.00016	160.06520±0.00047			160.06495±0.00025	s
	160.22085±0.00092	160.22112±0.00115	160.22098±0.00017	160.22072±0.00027	160.22092±0.00038	p
	160.37665±0.00048	160.37708±0.00046	160.37720±0.00077	160.37685±0.00055	160.37695±0.00029	s
	206.06571±0.00014	206.06514±0.00030	206.06573±0.00011	206.06516±0.00028	206.06544±0.00011	p
	206.22074±0.00027	206.22080±0.00006	206.22147±0.00018	206.22104±0.00024	206.22101±0.00010	s
J0121	109.26328±0.00016	109.26350±0.00031	109.26392±0.00032	109.26362±0.00074	109.26358±0.00022	s
	109.42392±0.00020	109.42385±0.00022	109.42398±0.00020	109.42387±0.00031	109.42391±0.00012	p
	110.23138±0.00015	110.23131±0.00008	110.23184±0.00048	110.23092±0.00017	110.23136±0.00013	s
	110.39235±0.00016	110.39241±0.00013	110.39241±0.00015	110.39220±0.00024	110.39234±0.00009	p
	112.32907±0.00027	112.32899±0.00016	112.32922±0.00014	112.32892±0.00017	112.32905±0.00010	p
	114.26625±0.00032	114.26654±0.00045	114.26641±0.00038	114.26616±0.00046	114.26634±0.00020	p
	114.42869±0.00019	114.42799±0.00023	114.42789±0.00012	114.42781±0.00027	114.42809±0.00010	s

Table 6 Eclipse Timings of J0254 and J0121.

Star	HJD(2400000+)	Error	E	$(O - C)_1$	$(O - C)_2$	Residual	Reference
J0254	53242.65066	0.00044	-18973.5	-0.00503	0.00067	-0.00287	(1)
	53246.70321	0.00083	-18960.5	-0.00700	-0.00130	-0.00483	(1)
	53993.67529	0.00136	-16565.5	-0.00141	0.00351	0.00210	(1)
	53994.60800	0.00134	-16562.5	-0.00436	0.00056	-0.00085	(1)
	53995.70804	0.00187	-16559.0	0.00408	0.00900	0.00759	(1)
	53997.57440	0.00082	-16553.0	-0.00087	0.00404	0.00264	(1)
	54003.65070	0.00105	-16533.5	-0.00635	-0.00144	-0.00283	(1)

Notes: (1)This paper (SuperWASP); (2)Yang et al. (2020); (3)ASAS-SN; (4)This paper (TESS); (5)This paper (NOWT). This table is available in its entirety in machine-readable form.

We fit $(O - C)$ diagrams with the OCFit package (Gajdoš & Parimucha 2019) in which the robust regression method was employed to achieve linear ephemeris fitting. The formula to indicate the linear ephemeris is as follows:

$$HJD = HJD_0 + P \times E. \quad (1)$$

3.1 J0254

For J0254, a total of eighty-one times of minima are determined, which are listed in Table 6. Based on the period of 0.3118858 days from the ASAS-SN database and all times of minima, the first linear ephemeris can be expressed as:

$$\begin{aligned} \text{Min.I} &= 2459160.22140 \text{ (9)} \\ &+ 0.31188613 \text{ (3)} \times E, \end{aligned} \quad (2)$$

The $(O - C)_2$ values based on this ephemeris plotted in the left panel of Fig. 2 suggests a continuously increasing period. A quadratic fit to these times of minima yields following ephemeris:

$$\begin{aligned} \text{Min.I} &= 2459160.22135 \text{ (5)} \\ &+ 0.31188673 \text{ (5)} \times E \\ &+ 4.2 \text{ (3)} \times 10^{-11} \times E^2, \end{aligned} \quad (3)$$

a continuous period increase ratio of $dP/dt = 9.8 \text{ (7)} \times 10^{-8} \text{ days yr}^{-1}$ is derived from the quadratic term.

3.2 J0121

We obtained forty-nine eclipse timings of J0121. With the period of 0.322819 days given by the ASAS-SN and all eclipse timings in Table 6, we derived the following linear ephemeris:

$$\begin{aligned} \text{Min.I} &= 2459109.42231 \text{ (54)} \\ &+ 0.32281773 \text{ (7)} \times E. \end{aligned} \quad (4)$$

The $(O - C)$ diagram plotted in the right panel of Fig. 2 clearly shows the signature of a linearly increasing period. The quadratic ephemeris was obtained as follows:

$$\begin{aligned} \text{Min.I} &= 2459109.42381 \text{ (19)} \\ &+ 0.32282331 \text{ (31)} \times E \\ &+ 3.1 \text{ (2)} \times 10^{-10} \times E^2, \end{aligned} \quad (5)$$

implying a continuous period increase of $dP/dt = 6.9 \text{ (4)} \times 10^{-7} \text{ days yr}^{-1}$.

For the two targets, we note that eclipse timings from Yang et al. (2020) did not correspond to the primary eclipse timings but secondary eclipse timings. The O-C analysis suggested that the orbital period of both targets is increasing, which will be discussed in Section 6.3.

4 CHROMOSPHERE ACTIVITY ANALYSIS

Chromospheric emission lines, including Ca II IRT, H_α , H_β , H_γ , H_δ , and Ca II H&K, are usually used to study whether late-type stars have chromospheric activity (Soderblom et al. 1993; Zhang et al. 2020). Our tar-

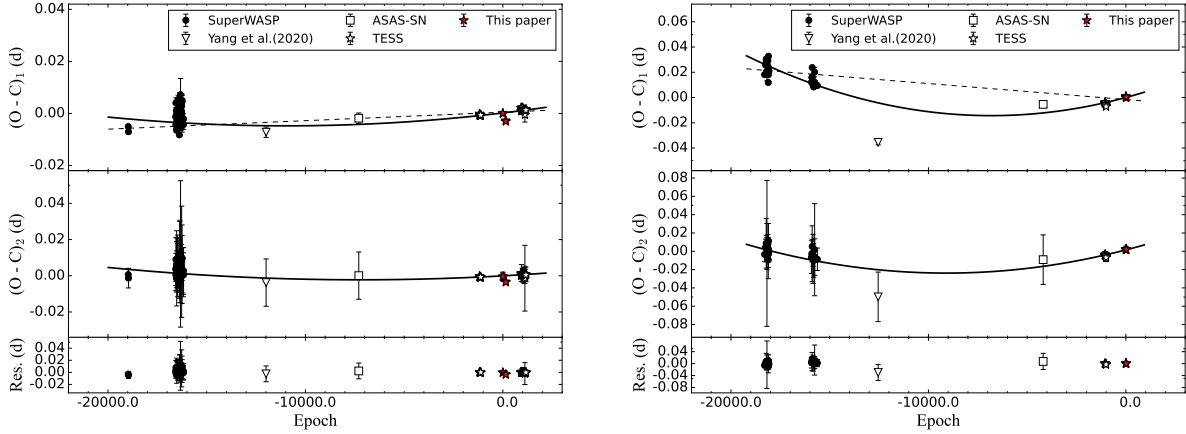


Fig. 2 $(O - C)$ diagrams for J0254 (left) and J0121 (right). The upper panel shows the $(O - C)_1$ data based on the initial information, with dotted lines represent linear fitting and solid lines indicate quadratic fitting. In the middle panel, $(O - C)_2$ is plotted using linear ephemeris to remove linear fitting $(O - C)_1$, the solid line shows a quadratic fitting for $(O - C)_2$, and the lower panel shows the quadratic fitting residuals for $(O - C)_2$.

gets J0254 and J0121 have 5 and 2 low-resolution spectra from LAMOST, respectively. The low-resolution spectra of binary is represented as a common characterization of its two components. The chromosphere activity emission lines of the binary are masked by its photosphere stronger absorption lines. So the spectral subtraction technique, whose principle is that stars with similar spectral types have nearly the same level of photospheric flux, is adopted in this paper to remove the influence of the photosphere. The chromospheric flux of active stars can be estimated by subtracting that of inactive stars with similar to the spectral types of the active stars (Montes et al. 1995).

Strassmeier et al. (2000) provided a list of 750 stars with no chromospheric activity. For these 750 sources, a total of fifty-two spectral lines were obtained from LAMOST DR7. There are thirty-nine spectral lines after removing poor spectral lines. The remaining lines were normalized to cross-match the seven spectral lines of the two targets, then obtained four spectra of HD 224844, HD 87680, and HD 13357. These four spectra were used to make synthetic spectra. The chromosphere activity signals of the two targets are detected by subtracting the synthesized spectra obtained from the spectra of the two targets. The results are shown in Fig. 3.

To evaluate these chromospherically active emission lines, we used the PHEW¹¹ package to calculate the equivalent widths (EWs) of these emission lines. The results obtained after a thousand MC iterations are listed in Table 7. Note that the low-resolution spectra are caused by the coupling of the two components of the two targets. Therefore, the spectral line broadening mechanism makes the equiv-

alent widths corresponding to these emission lines numerically small. The characteristics of the emission lines in Fig. 3 correspond essentially to their obtained equivalent widths, implying the presence of chromospheric activity in the both targets.

5 PHOTOMETRIC ANALYSIS

To further investigate J0254 and J0121, we analyzed our *BVRI* bands light curves by using the 2013 version of the W-D program (Wilson & Devinney 1971; Wilson 1979, 1990, 2008, 2012; Wilson et al. 2010). We set the effective temperature (T_1) of the primary star to be the average of the spectral temperatures in Table 1, 5544 ± 148 K for J0254 and 5659 ± 35 K for J0121. Based on this temperature, the gravity-darkening coefficients and the bolometric albedo were set to $g_{1,2} = 0.32$ (Lucy 1967) and $A_{1,2} = 0.5$ (Ruciński 1969) in the both targets. The bolometric and bandpass limb-darkening coefficients are estimated from van Hamme (1993) with the square-root functions law. Due to the lack of radial-velocity data for the two targets, we determined the mass ratios q of J0254 and J0121 by applying the q -search method to the NOWT data, and the results are shown in Fig. 4. We found the smallest $\sum \omega_i (O - C)_i^2$ obtained when $q = 0.72$ for J0254 and $q = 3.05$ for J0121 after using the W-D program.

When analyzing the light curve of a binary using the W-D program, we first need to determine the contact state of the two components of the binary system. But the contact states of these two targets cannot be determined yet. So we perform the calculation using mode 2, which corresponds to the detached binary. Then we found that the two components of the two targets always fill their Roche lobes during the process of operation, which means that the bina-

¹¹ Python Equivalent Widths <https://zenodo.org/record/47889>

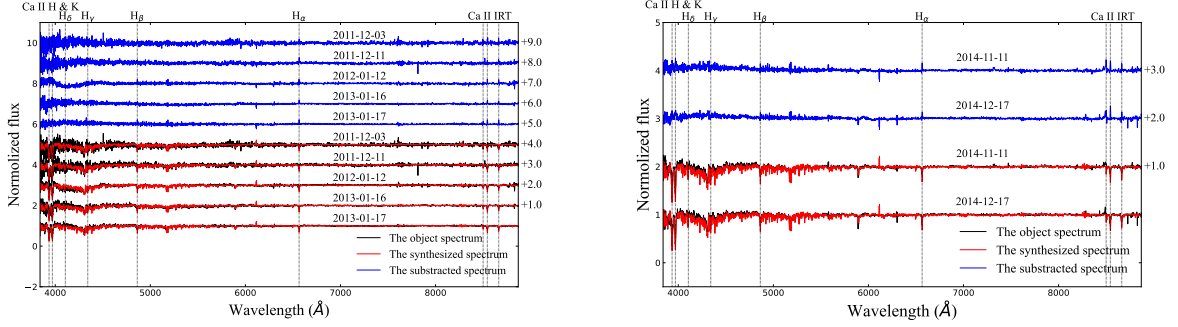


Fig. 3 The normalized object, synthesized and subtracted spectra for J0254 (left) and J0121 (right) observed by LAMOST. The excess emission lines are marked with dotted lines.

Table 7 The EWs of chromospheric activity indicators

Target	UT Date	Ca II K 3934.8Å	Ca II H 3969.6Å	H δ 4105.9Å	H γ 4341.7Å	H β 4862.7Å	H α 6564.6Å	Ca II IRT 18500.4Å	Ca II IRT 28544.4Å	Ca II IRT 38664.5Å
J0254	2011-12-03	2.05 ± 1.15	0.40 ± 0.35	0.34 ± 0.23	-	0.52 ± 0.24	0.70 ± 0.16	-	2.04 ± 0.57	1.19 ± 0.17
	2011-12-11	1.29 ± 0.53	0.57 ± 0.34	0.45 ± 0.37	0.50 ± 0.25	-	0.77 ± 0.12	0.66 ± 0.06	0.86 ± 0.24	1.44 ± 0.18
	2012-01-12	0.58 ± 0.34	1.21 ± 0.47	-	0.71 ± 0.12	0.62 ± 0.09	1.09 ± 0.15	1.09 ± 0.26	1.56 ± 0.18	1.39 ± 0.19
	2013-01-16	1.92 ± 0.66	0.90 ± 0.48	0.88 ± 0.39	0.28 ± 0.17	0.47 ± 0.17	0.74 ± 0.07	0.74 ± 0.18	1.26 ± 0.11	0.96 ± 0.14
J0121	2013-01-17	0.96 ± 0.36	1.24 ± 0.35	0.40 ± 0.06	0.55 ± 0.14	0.62 ± 0.14	1.15 ± 0.10	1.03 ± 0.25	1.87 ± 0.13	1.76 ± 0.24
	2014-11-11	0.51 ± 0.23	0.78 ± 0.33	0.30 ± 0.10	0.32 ± 0.07	0.45 ± 0.05	0.68 ± 0.11	1.31 ± 0.40	1.75 ± 0.20	1.10 ± 0.21
	2014-12-17	0.49 ± 0.53	0.53 ± 0.14	0.11 ± 0.10	0.18 ± 0.06	0.29 ± 0.03	0.43 ± 0.07	0.74 ± 0.46	1.66 ± 0.01	1.03 ± 0.27

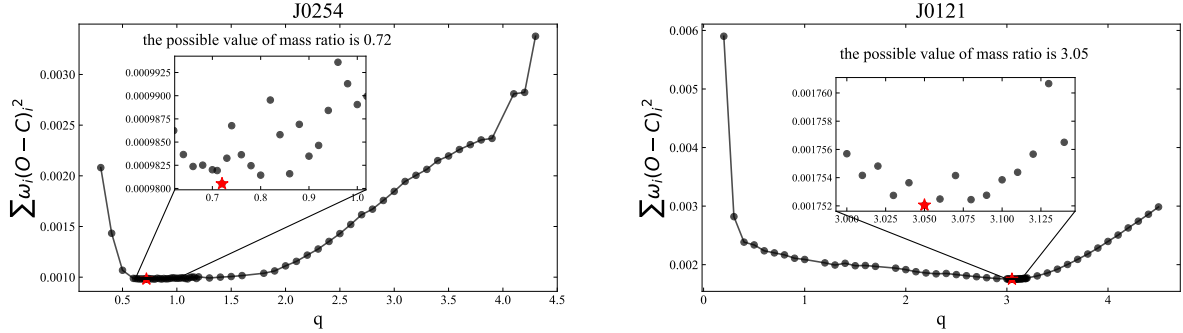


Fig. 4 Relationships between sum of squares of residuals $\sum \omega_i(O - C)_i^2$ and the mass ratios q for J0254 and J0121.

ries are the contact binaries (mode 3 in the W-D program). The adjustable parameters were the orbital inclination (i), the mean temperature of the secondary component (T_2), the monochromatic luminosity of the primary component (L_1) in each band of B , V , R , I , and the dimensionless potential ($\Omega_1 = \Omega_2$). The photometric elements of J0254 and J0121 are shown in Table 8. The results show that J0254 is a typical A-type W UMa contact binary, and J0121 is a W-type W UMa contact binary.

The O’Connell effect (difference in the maxima with 0.02 mag of J0254 in Fig. 5), classically thought of as an indicator of spot activity. For J0254, an excellent result can be obtained by adding a cold spot to the main component. The results are shown in Table 8 and the theoretical light curves with and without spots are displayed in the left half of Fig. 5. We note that $\sum W(O - C)^2$ of 0.0017 acquired with the cool spot is smaller than $\sum W(O - C)^2 = 0.0020$

without starspot for J0254. According to the NOWT data, we found no evidence of the presence of starspot on J0121.

We also performed the photometric analysis of CRTS, ASAS-SN, and ZTF data. Considering that the photometric light curve of CRTS and ASAS-SN was obtained at similar observation time of LAMOST spectra (from 2011 to 2014), we adopted the spot model to fit these light curves, as well as the same input parameters mentioned above. When running the program, in order to simplify the model, the spot latitude ϕ is fixed at 90° (1.5708 *radian*) and the temperature factor $T_f (T_d/T_0)$ is fixed at 0.8. We found the presence of a cold spot on the more massive component of J0254 based on the ASAS-SN data, but no starspot is present in the CRTS with ZTF data results. While the results of J0121 in CRTS, ASAS-SN, and ZTF data all indicate the presence of a cold spot on its massive component. The optimal results are presented in Table 9, and the

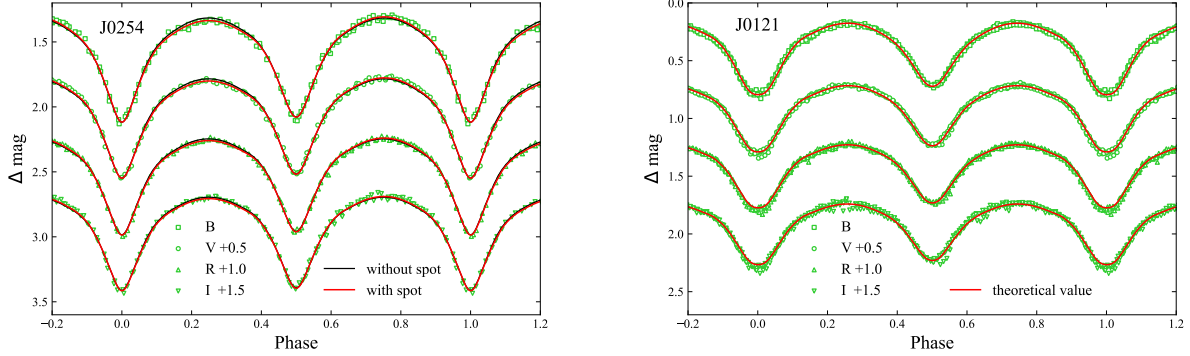


Fig. 5 Theoretical and observed light curves of J0254 and J0121 obtained in this paper.

Table 8 Photometric Elements of J0254 and J0121

Parameters	J0254		J0121	
	Values	Errors	Values	Errors
$g_1 = g_2$	0.32	Assumed	0.32	Assumed
$A_1 = A_2$	0.5	Assumed	0.5	Assumed
Ω_{in}	3.27848	Assumed	6.68243	Assumed
Ω_{out}	2.86696	Assumed	6.06275	Assumed
$q(M_2/M_1)$	0.72	± 0.001	3.05	± 0.0022
$T_1(K)$	5544	± 148.12	5659	± 35.13
$T_2(K)$	5529	± 7.73	5448	± 3.46
i°	82.641	± 0.17	79.099	± 0.095
$\Omega_1 = \Omega_2$	3.23888	0.00368	6.61727	0.00385
L_{1B}/L_B	0.5782	± 0.0024	0.3194	± 0.0009
L_{1V}/L_V	0.5772	± 0.0019	0.3061	± 0.0007
L_{1R}/L_R	0.5766	± 0.0019	0.2982	± 0.0006
L_{1I}/L_I	0.5762	± 0.0021	0.2925	± 0.0006
r_1 (pole)	0.3893	± 0.0005	0.2720	± 0.0003
r_1 (side)	0.4119	± 0.0007	0.2840	± 0.0003
r_1 (back)	0.4442	± 0.0009	0.3200	± 0.0005
r_2 (pole)	0.3348	± 0.0005	0.4531	± 0.0003
r_2 (side)	0.3513	± 0.0007	0.4870	± 0.0003
r_2 (back)	0.3866	± 0.0010	0.5141	± 0.0004
f	9.62 %	$\pm 0.89\%$	10.52 %	$\pm 0.62\%$
θ (radian)	4.8184	± 0.0690	-	-
ϕ (radian)	1.5708	± 0.2875	-	-
r (radian)	0.2203	± 0.0080	-	-
$T_f(T_d/T_0)$	0.8196	± 0.0179	-	-

fitted theoretical light curves are plotted in Fig. 6. The corresponding stellar structure is presented in Fig. 7.

As shown in the above results, from the CRTS and ZTF data, no starspot was found on J0254. This may be due to the fact that the two components of J0254 have similar masses, so that the chances of magnetic activity occurring in either component may be equal, which makes the dispersion increase at the two maxima of the light curve, thus masking the starspot. In conclusion, the photometric solutions for J0254 and J0121 indicate the presence of starspots. Combined with our chromospheric activity analysis, it is confirmed that the two targets have magnetic activity.

6 DISCUSSION

In this section, we discussed absolute parameters estimation with different methods (Section 6.1), calculated the distances of the two targets (Section 6.2), and analyzed the evolution for our targets (Section 6.3).

6.1 Absolute parameters

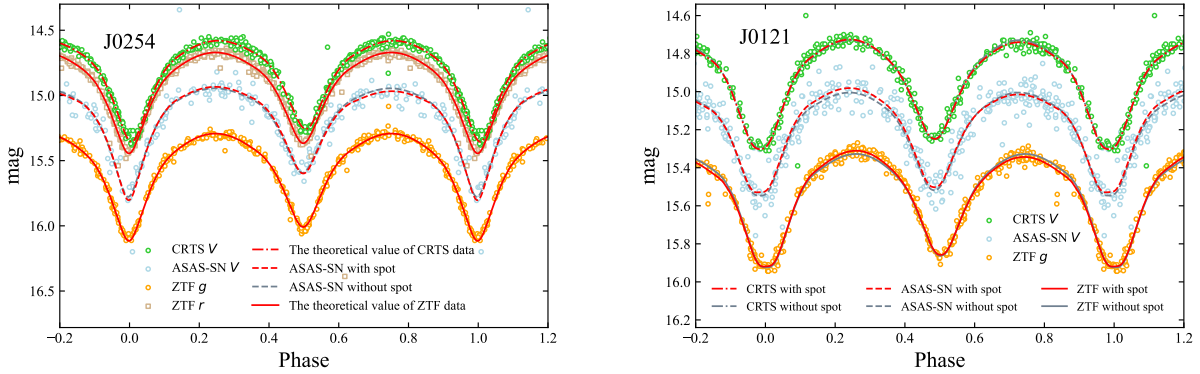
The absolute parameters of binary usually include mass M , radius R , luminosity L , and the semi-major axis of the orbit a . These parameters are linked to each other. In a binary system, the accurate absolute parameters can be determined in the case of having radial-velocity curves. However, in the absence of the radial-velocity curves, we can only use some estimation methods to assess the absolute parameters of the binary system.

Zhang et al. (2017) proposed a new method for estimating absolute parameters and provided mass-radius relations of two contact binary systems (GQ Boo and V1367 Tau). They obtained the approximate masses and radii by using the relations to limit the almost complete stellar parameter space provided by PARSEC¹² (Bressan et al. 2012), which include all the initial stellar masses ($0.1 < M(M_\odot) < 350$) and ages ($6.6 < \log(t/\text{yr}) < 10.13$), the metallicity $Z = 0.010-0.023$ are selected for GQ Boo, and $Z = 0.0001-0.0700$ for V1367 Tau. They pointed out that the more massive components are more suitable than the less massive components for matching the absolute parameters, with the temperature of 200K error being used to limit the more massive components. They also pointed out that single stars are brighter and hotter than components of the same mass in a contact binary system, that there may be some bias in the estimates using the single-star evolution procedure, and that the PARSEC program may be more applicable to detached binaries. The method is used to con-

¹² PAdova and Trieste Stellar Evolution Code <http://stev.oapd.inaf.it/cgi-bin/cmd>

Table 9 Photometric Elements of J0254 and J0121 based on survey data

Parameters	J0254			J0121		
	CRTS	ASAS-SN	ZTF	CRTS	ASAS-SN	ZTF
$q(M_2/M_1)$	0.72	0.72	0.72	3.05	3.05	3.05
$T_1(K)$	5544	5544	5544	5659	5659	5659
$T_2(K)$	5410 ± 17.59	5287 ± 94.10	5430 ± 18.42	5436 ± 35.71	5498 ± 64.85	5442 ± 16.38
i°	81.859 ± 0.267	84.044 ± 1.707	82.345 ± 0.304	79.028 ± 0.627	80.162 ± 1.573	79.953 ± 0.442
$\Omega_1 = \Omega_2$	3.2486 ± 0.0078	3.2776 ± 0.0303	3.2268 ± 0.0080	6.6178 ± 0.0253	6.6715 ± 0.0479	6.6115 ± 0.0167
L_{1V}/L_V	0.6049 ± 0.0041	0.5772 ± 0.0231	-	0.3086 ± 0.0072	0.2937 ± 0.0125	-
L_{1g}/L_g	-	-	0.6037 ± 0.0053	-	-	0.3148 ± 0.0040
L_{1r}/L_r	-	-	0.5960 ± 0.0038	-	-	-
$r_1(pole)$	0.3880 ± 0.0010	0.3835 ± 0.0043	0.3913 ± 0.0012	0.2724 ± 0.0018	0.2676 ± 0.0033	0.2725 ± 0.0012
$r_1(side)$	0.4102 ± 0.0014	0.4046 ± 0.0054	0.4143 ± 0.0015	0.2844 ± 0.0021	0.2786 ± 0.0038	0.2845 ± 0.0014
$r_1(back)$	0.4418 ± 0.0020	0.4342 ± 0.0072	0.4475 ± 0.0020	0.3207 ± 0.0035	0.3112 ± 0.0061	0.3209 ± 0.0024
$r_2(pole)$	0.3333 ± 0.0012	0.3291 ± 0.0044	0.3366 ± 0.0012	0.4531 ± 0.0017	0.4496 ± 0.0031	0.4535 ± 0.0011
$r_2(side)$	0.3496 ± 0.0014	0.3445 ± 0.0053	0.3535 ± 0.0015	0.4869 ± 0.0022	0.4822 ± 0.0042	0.4875 ± 0.0015
$r_2(back)$	0.3839 ± 0.0021	0.3764 ± 0.0076	0.3899 ± 0.0022	0.5141 ± 0.0028	0.5081 ± 0.0052	0.5148 ± 0.0019
$spot$	-	primary star	-	secondary star	secondary star	secondary star
f	$5.29\% \pm 1.90\%$	$0.22\% \pm 7.36\%$	$12.55\% \pm 1.94\%$	$10.43 \pm 4.08\%$	$1.76 \pm 7.72\%$	$11.45 \pm 2.70\%$
$\theta(radian)$	-	1.7078 ± 0.6222	-	4.9995 ± 0.5052	4.6397 ± 0.3150	4.5441 ± 0.0903
$\phi(radian)$	-	1.5708	-	1.5708	1.5708	1.5708
$r(radian)$	-	0.2380 ± 0.0678	-	0.1491 ± 0.0336	0.2233 ± 0.0325	0.2146 ± 0.0115
$T_f(T_d/T_0)$	-	0.8	-	0.8	0.8	0.8

**Fig. 6** Theoretical and observed light curves of J0254 and J0121 obtained from CRTS, ASAS-SN, ZTF.

tact binaries resulting in biases that are within the errors of the absolute parameters obtained. The setting of the atmospheric input parameters has the most influence on this method.

Wang et al. (2019) provided a method depending on the calculation of the Roche lobes (the DCRL method), while referring to the method used by Zhang et al. (2017) as DCWD, which depends on the stellar radius obtained from the W-D code. In their paper, these two methods are used to obtain the absolute parameters of AL Cas.

Lu et al. (2020) provided a general formula for the DCRL method suitable for any contact binary system. The DCRL method assumes that the radius of the companion star coincides with the effective radius of the Roche lobe R_L that can be obtained by the following relation (Eggleton 1983):

$$\frac{R_L}{a} = \frac{0.49q^{2/3}}{0.6q^{2/3} + \ln(1 + q^{1/3})}, \quad (6)$$

where q is mass ratio, $q = M_1/M_2$ for R_{L1} and $q = M_2/M_1$ for R_{L2} .

According to Equation (6), the mass-radius relation of DCRL was derived as:

$$\frac{R}{R_\odot} = 2.0627 \left[\frac{q^{1/3} p^{2/3} (q+1)^{1/3}}{0.6q^{2/3} + \ln(1 + q^{1/3})} \right] \left(\frac{M}{M_\odot} \right)^{1/3}, \quad (7)$$

where $0 < q < 1$, and P is the orbital period. The star parameter space is obtained by PARSEC v1.2S stellar evolution code, and the parameters are listed in Table 10. They tested 140 binary systems (76 W-type and 64 A-type systems) with sufficient spectral information and found that their method is suitable for short-period W UMa systems with a high mass ratio and low effective temperature. Since the fractional difference $\left(\frac{Mass_{Av=0} - Mass_{Av \neq 0}}{Mass_{Av=0}} \right)$ for all sets of parameters is found less than 2.4%, A_v was set as 0 by them.

In this paper, we provide a generic formulation for the DCWD method that can be used for any contact binary and requires only some of the parameters of that binary system. Combining Equation (6) with Kepler's third law, we obtain

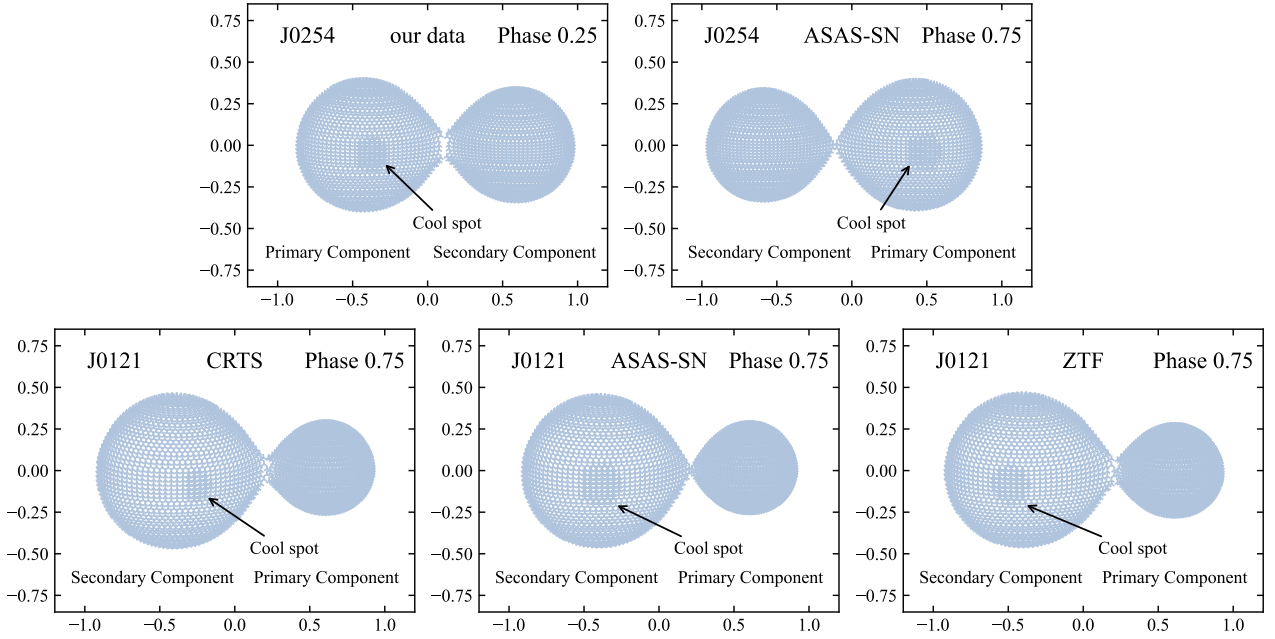


Fig. 7 Stellar configuration and spot distribution for J0254 and J0121.

Table 10 Parameter space of PARSEC.

Name	Parameter space	Reference
Evolutionary tracks	PARSEC version 1.2S	1,2,3
Photometric systems	<i>UBVR</i> <i>IJK</i>	4,5,6
Circumstellar dust	No dust	7
Mass	$0.1 M_{\odot} < M < 350 M_{\odot}$	1,2
Age	$6.6 < \log(t) < 10.13$	1,2
Metallicities	$0.0001 < Z < 0.07$	1,2
Interstellar extinction	$R_v = 3.1, A_v = 0$	8,9

Notes: 1 Tang et al. (2014); 2 Chen et al. (2015); 3 Chen et al. (2014); 4 Maíz Apellániz (2006); 5 Bessell (1990); 6 Bessell & Brett (1988); 7 Marigo et al. (2008); 8 Cardelli et al. (1989); 9 O’Donnell (1994).

the mass-radius relationship:

$$\frac{R}{R_{\odot}} = \frac{2.4089(1+q)^{1/3} P^{2/3} r}{q^{1/3}} \left(\frac{M}{M_{\odot}} \right)^{1/3}, \quad (8)$$

where $0 < q < 1$, and r is the result of the ratio of the companion radius to the semi-major axis of orbit obtained by the photometric analysis using the W-D program.

The mass-radius relations J0254 and J0121 are obtained from the orbital period P , the mass ratio q , the ratio of radius and semi-major axis $r = R/a$ and Equations (7) and (8).

For J0254,

$$\frac{M_1}{M_{\odot}} = 0.84550(\pm 0.00027) \left(\frac{R_1}{R_{\odot}} \right)_{DCRL}^3, \quad (9)$$

$$\frac{M_1}{M_{\odot}} = 0.88897(\pm 0.00355) \left(\frac{R_1}{R_{\odot}} \right)_{DCWD}^3.$$

For J0121,

$$\frac{M_2}{M_{\odot}} = 1.12407(\pm 0.00025) \left(\frac{R_2}{R_{\odot}} \right)_{DCRL}^3, \quad (10)$$

$$\frac{M_2}{M_{\odot}} = 1.17083(\pm 0.00443) \left(\frac{R_2}{R_{\odot}} \right)_{DCWD}^3.$$

In this work, we use the PARSEC program of CMD version 3.6. For its input parameter space, there are three considerations.

1. In case 1, the complete parameter space without restriction. The circumstellar dust is chosen for “No dust” mode, all the initial stellar masses ($0.1 < M (M_{\odot}) < 350$) are used. The evolution model settings use the default values. The metallicity Z from 0.0001 to 0.06 in steps of 0.0001 and the logarithmic age from 6.6 to 10.13 in steps of 0.05.
2. In case 2, since Yıldız (2014) indicated that the average age of W UMa systems is around 4.4–4.6 Gyr, it varies depending on type A or W, so we limit the input to ages above 10^8 . The age with logarithmic from 8 to 10.13 in steps of 0.05, other input parameters are the same as in case 1.
3. In case 3, the logarithmic age from 8 to 10.13 in steps of 0.01, and the step of metallicity Z is 0.0001. Here, $0.0063 < Z < 0.0170$ for J0254 and $0.0080 < Z < 0.0109$ for J0121 are used, and the metallicity is derived from low-resolution spectra of LAMOST. Other input parameters are the same as in case 1.

We floated the temperature at 300 K to constrain the PARSEC output parameters. Using the DCWD method in case 1 as an example, the results of the two targets are shown in Fig. 8. Data within a triple error margin of the mass-radius relationship for both targets were used to estimate the approximate absolute parameters (mass and radius) for the more massive component. We also calculated other absolute parameters and all results are presented in Table 11.

From the results, when the parameter input space of the PARSEC program was constrained by age, the maximum range of variation of the absolute parameters was 2.8%. The parameters of the two targets have different responses for the age constraint in case 1 and case 2. From the assumptions of case 1 and case 2, the age space changes from $6.6 < \log(t/\text{yr}) < 10.13$ to $8.0 < \log(t/\text{yr}) < 10.13$, and the estimated parameters of J0254 decrease while those of J0121 remain the same or even increase slightly when using the DCRL method. In contrast, when using the DCWD method, the estimated parameters of J0254 are unchanged and those of J0121 are decreased. This situation may be due to the difference in the mass ratio of the two targets, or the difference in the models, which may require more target samples to analyze the causes. The results change significantly from case 2 to case 3, where we overestimate the absolute parameters of the targets by about 10-15% without considering metallicity, which may be caused by the reduction of the parameter space making very few data satisfying the mass-radius relationship. The absolute parameter estimation method combined with the PARSEC stellar evolution model would underestimate the parameters of the target, since the more massive part of the binary is fainter and cooler than a single star with the same mass. Thus, it is closer to the actual value without restricting the atmospheric parameters. Combining the radial velocity profiles could yield physical parameters that approximate the actual values. Therefore, it is necessary to obtain radial velocity profiles by additional spectroscopic observations.

6.2 Distances

Using the DCRL with DCWD method, the obtained luminosity of the more massive component of our targets J0254 and J0121 are applied to the calculation of distances. The formula used for this calculation is as follows: (a) $-2.5 \log(L/L_\odot) = M_{bol} - 4.73$ (Torres 2010), (b) $M_{bol_i} = M_{V_i} + BC_{V_i}$, (c) $m_{V_i} - m_{V_{max}} = -2.5 \log(L_i/L)$, (d) $M_{V_i} = m_{V_i} - 5 \log D + 5 - A_V$. During the calculation, some parameters are necessary, including the interstellar extinction coefficient $A_{v_{S\&F}}$

(Schlafly & Finkbeiner 2011) from IRSA database¹³ ($A_v = 0.367$ for J0254 and $A_v = 0.226$ for J0121), the bolometric corrections from Pecaut & Mamajek (2013) ($BC_V = -0.126$ for J0254 and $BC_V = -0.146$ for J0121), and the maximum visual magnitude $m_{V_{max}}$ obtained by fitting ASAS-SN data ($m_{V_{max}} = 14.945$ mag for J0254 and $m_{V_{max}} = 15.005$ mag for J0254). The results are listed in Table 12. In order to verify the reliability of the parameter estimation method we used and the distances obtained, we used the distances provided by Bailer-Jones et al. (2018) (hereafter BJ18), the photometric distances provided by Bailer-Jones et al. (2021) (hereafter BJ21) and the distances obtained from Gaia DR3 (Gaia Collaboration 2022) for comparison with the distances we obtained.

By comparison, we find that the obtained distances are in general agreement with the distances in the literature, which proves the validity of the method we adopted. From the results, the parameters obtained in case 1 may be closer to the actual values.

6.3 Mass transfer and evolution of angular momentum

In this section, we use the absolute parameters obtained by the DCWD method in the case 1 condition (see table 11) to study the evolution of the two targets.

The ($O - C$) analysis shows that for both J0254 and J0121, there is a long-term trend of increasing orbital periods for both systems. This phenomenon can be explained by mass transfer. The equation ($\dot{P} = 3\dot{M}_1 \left(\frac{1}{M_2} - \frac{1}{M_1} \right)$) given by Tout & Hall (1991) was used to calculate the mass transfer rate of binary. The mass transfer rates of our two targets were obtained, with J0254 ($dM_1/dt = 2.682 \times 10^{-7} M_\odot \text{ yr}^{-1}$) and J0121 ($dM_1/dt = -3.603 \times 10^{-7} M_\odot \text{ yr}^{-1}$). From the mass transfer rates and the mass ratio of the two targets, we suggested that both targets are transferring mass from the less massive components to the more massive components. This means that these two targets are potentially excellent targets for proving the theory of thermal relaxation oscillations (Lucy 1967; Lucy & Wilson 1979). Mass transfer from lower to higher mass components in the W UMa system leads to an increase in the orbital angular momentum. According to the thermal relaxation oscillation model, these two targets may evolve as semi-detached binaries. Our two targets have magnetic activity, so the possibility that magnetic activity plays a role in the orbital period variation cannot be denied. However, due to the insufficient accumulation of occultation times, further studies of the orbital period variation of these two targets are needed in the future.

¹³ <https://irsa.ipac.caltech.edu/applications/DUST/>

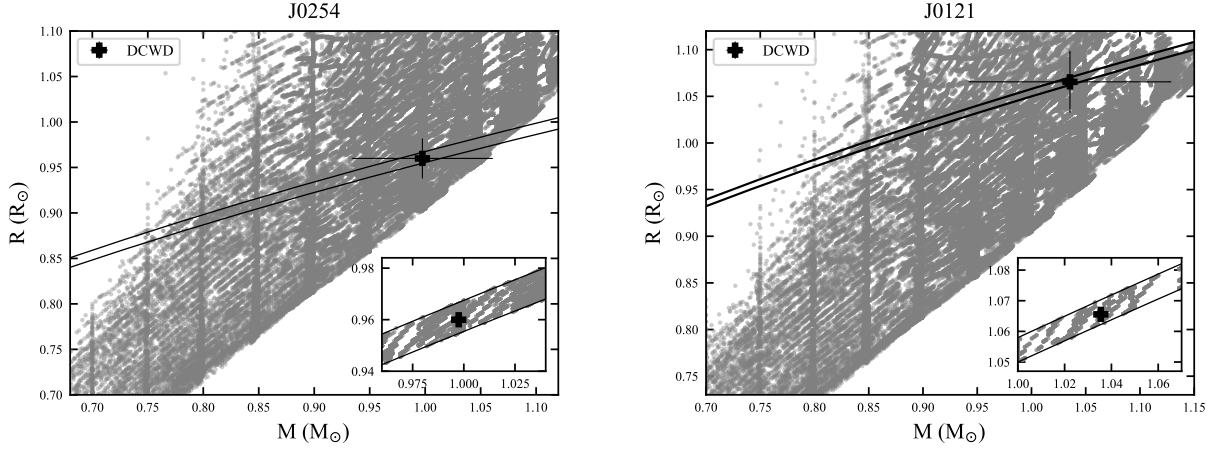


Fig. 8 The stellar M-R relation of J0254 and J0121 using the DCWD method in case 1.

Table 11 The absolute parameters of J0254 and J0121 are obtained by using DCRL and DCWD methods.

Object	Model	DCRL			DCWD		
		case 1	case 2	case 3	case 1	case 2	case 3
J0254	$M_1(M_\odot)$	0.988 ± 0.068	0.963 ± 0.062	0.900 ± 0.058	0.998 ± 0.063	0.997 ± 0.059	0.909 ± 0.062
	$M_2(M_\odot)$	0.711 ± 0.049	0.693 ± 0.045	0.648 ± 0.042	0.718 ± 0.046	0.718 ± 0.044	0.654 ± 0.046
	$R_1(R_\odot)$	0.941 ± 0.022	0.933 ± 0.021	0.913 ± 0.020	0.960 ± 0.021	0.960 ± 0.020	0.931 ± 0.022
	$R_2(R_\odot)$	0.810 ± 0.250	0.803 ± 0.247	0.785 ± 0.241	0.827 ± 0.021	0.827 ± 0.020	0.801 ± 0.022
	$\alpha(R_\odot)$	2.309 ± 0.394	2.289 ± 0.388	2.239 ± 0.378	2.316 ± 0.054	2.316 ± 0.052	2.245 ± 0.056
	$L_1(L_\odot)$	0.750 ± 0.115	0.737 ± 0.112	0.705 ± 0.106	0.780 ± 0.117	0.780 ± 0.116	0.733 ± 0.112
	$L_2(L_\odot)$	0.549 ± 0.342	0.540 ± 0.335	0.517 ± 0.320	0.572 ± 0.033	0.572 ± 0.031	0.538 ± 0.032
	$M_1(M_\odot)$	0.335 ± 0.026	0.336 ± 0.026	0.281 ± 0.003	0.339 ± 0.031	0.330 ± 0.027	0.281 ± 0.007
J0121	$M_2(M_\odot)$	1.020 ± 0.079	1.024 ± 0.079	0.856 ± 0.010	1.035 ± 0.092	1.006 ± 0.081	0.858 ± 0.021
	$R_1(R_\odot)$	0.630 ± 0.166	0.631 ± 0.166	0.595 ± 0.143	0.641 ± 0.021	0.635 ± 0.018	0.603 ± 0.006
	$R_2(R_\odot)$	1.046 ± 0.027	1.047 ± 0.027	0.987 ± 0.004	1.066 ± 0.032	1.055 ± 0.029	1.001 ± 0.009
	$\alpha(R_\odot)$	2.191 ± 0.346	2.193 ± 0.346	2.067 ± 0.280	2.201 ± 0.068	2.180 ± 0.061	2.069 ± 0.020
	$L_1(L_\odot)$	0.365 ± 0.201	0.366 ± 0.201	0.325 ± 0.164	0.378 ± 0.034	0.371 ± 0.031	0.334 ± 0.015
	$L_2(L_\odot)$	0.864 ± 0.047	0.866 ± 0.047	0.769 ± 0.008	0.896 ± 0.056	0.879 ± 0.050	0.792 ± 0.016

Table 12 Distances of J0254 and J0121.

Source	Distance(pc)	
	J0254	J0121
BJ18 ¹	1093 ± 49	1177 ± 56
BJ21 ²	1045 ± 38	1205 ± 47
Gaia DR3 ³	1091 ± 34	1149 ± 44
DCRL <i>case 1</i>	1003 ± 135	1067 ± 101
DCRL <i>case 2</i>	994 ± 133	1068 ± 101
DCRL <i>case 3</i>	973 ± 130	1007 ± 72
DCWD <i>case 1</i>	1023 ± 136	1087 ± 107
DCWD <i>case 2</i>	1023 ± 135	1076 ± 103
DCWD <i>case 3</i>	992 ± 133	1022 ± 79

Notes: 1 Bailer-Jones et al. (2018); 2 Bailer-Jones et al. (2021); 3 Gaia Collaboration (2022).

To compare with earlier studies, we used Table 7 of Li et al. (2021), including 94 A-type systems and 85 W-type systems, to understand the evolutionary state of our two contact binaries. The M-R (mass-radius) and M-L (mass-luminosity) relations are plotted in Fig. 9. As seen in the figure, in most binary systems, including both targets, the more massive part is closer to the ZAMS than the less massive part, which is different from our perception that the more massive single stars evolve faster. This phenomenon can be explained by two conjectures, one being

that mass transfer leads to the mass ratio reversal (Guinan & Bradstreet 1988), and the other is the theory of thermal relaxation oscillations, where the transfer of energy from the massive component to the less massive component increases the radius and luminosity of the less massive component, and makes its own radius and luminosity decrease. J0254 is more suitable for the second conjecture explanation, while the lower-mass component of J0121 has evolved faster and has left TAMS. Therefore, J0121 is more suitable for the first explanation, the current lower-mass component is the initially higher-mass component of the binary system, and this component underwent a rapid mass transfer process when it left the main sequence phase.

The ratio of the spin angular momentum J_{spin} to the orbital angular momentum J_{orb} reflects the stability of the binary evolution. When $J_{\text{spin}}/J_{\text{orb}} < 1/3$, the binary is in a relatively stable evolutionary state. Yang & Qian (2015) provided the equation $\frac{J_{\text{spin}}}{J_{\text{orb}}} = \frac{1+q}{q} \left[(k_1 r_1)^2 + (k_2 r_2)^2 \right] q$ which allows calculate this ratio, where r_i is ratio of the radius R_i to the semi-major axis of the orbit a , and the value of k_i^2 is set as 0.06 (Li & Zhang 2006). According to the above equation, we obtained the ratio of the spin angu-

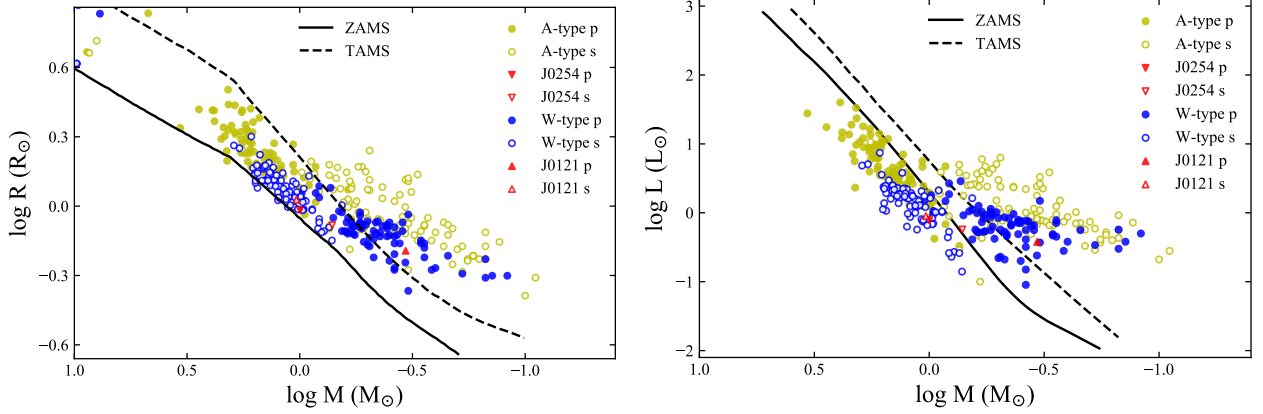


Fig. 9 The mass-radius diagram (left) and mass-luminosity diagram (right). The solid line represents the zero-age main sequence (ZAMS), and the terminal-age main sequence (TAMS) is expressed as a dashed line. The two lines are constructed by the binary system evolution code provided by Hurley et al. (2002). Red represents our own two targets, with J0254 in regular triangles, and J0121 in inverted triangles. The A-type contact binaries and the W-type contact binaries from Li et al. (2021) are also displayed as yellow circles and blue circles, respectively. In addition, solid triangles represent the primary components with the high temperature, which are represented by p.

lar momentum J_{spin} to the orbital angular momentum J_{orb} for the two targets as 0.0378 (J0254) and 0.0637 (J0121), respectively. The results indicate that J0254 and J0121 are currently in a stable evolutionary state.

Eker et al. (2006) provided the correlation between the contact state and the orbital angular momentum of the binary. To investigate the contact state of the two targets, we calculate the orbital angular momentum with the equation $J_{\text{orb}} = 1.24 \times 10^{52} \times M^{5/3} \times P^{1/3} \times q \times (1 + q)^{-2}$ given by Christopoulou & Papageorgiou (2013), where M is the total mass of the system. The orbital angular momentums of our two targets were obtained, with 51.702 (J0254) and 51.429 (J0121). The relationship between $\log J_{\text{orb}}$ and $\log M$ of two targets are shown in Fig. 10. It can be seen that J0121 is a contact binary, while J0254 is a shallow contact binary, which may have evolved from short-period detached binaries by angular momentum loss.

7 SUMMARY

We performed new photometric observations of J0254 and J0121 using NOWT. We analyzed the chromospheric activity of the two targets based on LAMOST spectroscopic data. Combining the photometric data from NOWT and the survey database, we provided the linear ephemeris of the two targets, studied their orbital period variations, and also analyzed the light curves of the two targets. We also discuss various absolute parameter estimation methods and apply them to two targets to obtain their absolute parameters. In this paper, we compare the distances of the targets with those in the literature by calculating them.

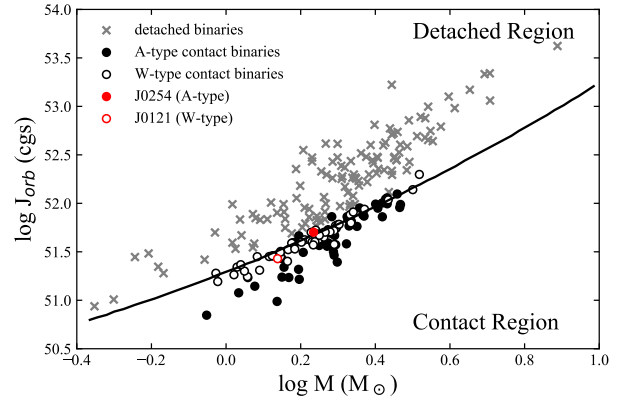


Fig. 10 The mass and the orbital angular momentum diagram. The detached binaries, the A-type contact binaries and the W-type contact binaries from Eker et al. (2006) are shown as crosses in gray, black solid circles and black hollow circles, respectively. The border line in solid black, which separates the detached and contact systems, is also found by Eker et al. (2006). The red circles represent our targets.

1. According to the results of the light curve analysis, J0254 is a typical A-type W UMa contact binary, and J0121 is a W-type W UMa contact binary.
2. The results show the presence of stellar spots with chromospheric activity in both targets, which indicates the presence of magnetic activity in J0254 and J0121.
3. The ($O - C$) analysis shows that both J0254 and J0121 exhibit a long-term increasing trend in their orbital periods, implying that both targets are transferring mass

from their less massive companions to their more massive ones.

4. We also studied the evolutionary status of these two targets and found that both of them are in the evolutionary stability stage. Based on the thermal relaxation oscillation theory, we predict that these two targets will transition from the contact state to the semi-detached state.

Acknowledgements We thank the anonymous referee very much for the very helpful comments. This work received the generous support of the National Natural Science Foundation of China under grants U2031204. We gratefully acknowledge the science research grants from the China Manned Space Project with NO.CMSCSST-2021-A08. We acknowledge the support of the staff of the Nanshan One-meter Wide-field Telescope (NOWT). The spectral data were provided by Guoshoujing Telescope (the Large Sky Area Multi-Object Fiber Spectroscopic Telescope, LAMOST). LAMOST is operated and managed by the National Astronomical Observatories, Chinese Academy of Sciences. This work includes data collected by the CRTS mission, ASAS-SN mission and ZTF mission. This paper makes use of data from the DR1 of the WASP data (Butters et al. 2010) as provided by the WASP consortium, and computational resources supplied by the project "e-Infrastruktura CZ" (e-INFRA CZ LM2018140) supported by the Ministry of Education, Youth and Sports of the Czech Republic. This research has made use of the International Variable Star Index (VSX) database, operated at AAVSO, Cambridge, Massachusetts, USA. This work has made use of data from the European Space Agency (ESA) mission *Gaia* (<https://www.cosmos.esa.int/gaia>), processed by the *Gaia* Data Processing and Analysis Consortium (DPAC, <https://www.cosmos.esa.int/web/gaia/dpac/consortium>). Funding for the DPAC has been provided by national institutions, in particular the institutions participating in the *Gaia* Multilateral Agreement. This research also has made use of the SIMBAD database, operated at CDS, Strasbourg, France, NASA Astrophysics Data System Abstract Service. Funding for the TESS mission is provided by NASA's Science Mission directorate. This research made use of Lightkurve, a Python package for Kepler and TESS data analysis (Lightkurve Collaboration et al. 2018).

Software: Lightkurve (Lightkurve Collaboration et al. 2018), Astropy (Astropy Collaboration et al. 2013, 2018), Astroquery (Ginsburg et al. 2019), Tesscut (Brasseur et al. 2019), Numpy (Harris et al. 2020), Matplotlib (Hunter 2007), OCFit (Gajdoš & Parimucha 2019), PHEW (Alam & Douglas 2016), PARSEC (v1.2s Bressan et al. 2012), IRAF (Tody 1986, 1993)

References

- Alam, M., & Douglas, S. 2016, PHEW: PytHon Equivalent Widths 14
- Applegate, J. H. 1992, ApJ, 385, 621 1
- Astropy Collaboration, Robitaille, T. P., Tollerud, E. J., et al. 2013, A&A, 558, A33 14
- Astropy Collaboration, Price-Whelan, A. M., Sipőcz, B. M., et al. 2018, AJ, 156, 123 14
- Bai, C.-H., Feng, G.-J., Zhang, X., et al. 2020, Research in Astronomy and Astrophysics, 20, 211 2
- Bailer-Jones, C. A. L., Rybizki, J., Fouesneau, M., Demleitner, M., & Andrae, R. 2021, AJ, 161, 147 11, 12
- Bailer-Jones, C. A. L., Rybizki, J., Fouesneau, M., Mantelet, G., & Andrae, R. 2018, AJ, 156, 58 11, 12
- Bellm, E. C., Kulkarni, S. R., Graham, M. J., et al. 2019, PASP, 131, 018002 1
- Bessell, M. S. 1990, PASP, 102, 1181 10
- Bessell, M. S., & Brett, J. M. 1988, PASP, 100, 1134 10
- Binnendijk, L. 1970, Vistas in Astronomy, 12, 217 1
- Borkovits, T., Elkhateeb, M. M., Csizmadia, S., et al. 2005, A&A, 441, 1087 1
- Brasseur, C. E., Phillip, C., Fleming, S. W., Mullally, S. E., & White, R. L. 2019, Astrocut: Tools for creating cutouts of TESS images, Astrophysics Source Code Library, record ascl:1905.007 14
- Bressan, A., Marigo, P., Girardi, L., et al. 2012, MNRAS, 427, 127 8, 14
- Butters, O. W., West, R. G., Anderson, D. R., et al. 2010, A&A, 520, L10 1
- Cardelli, J. A., Clayton, G. C., & Mathis, J. S. 1989, ApJ, 345, 245 10
- Chen, Y., Bressan, A., Girardi, L., et al. 2015, MNRAS, 452, 1068 10
- Chen, Y., Girardi, L., Bressan, A., et al. 2014, MNRAS, 444, 2525 10
- Christopoulou, P. E., & Papageorgiou, A. 2013, AJ, 146, 157 13
- Cutri, R. M., Skrutskie, M. F., van Dyk, S., et al. 2003, VizieR Online Data Catalog, II/246 3
- Drake, A. J., Djorgovski, S. G., Mahabal, A., et al. 2009, ApJ, 696, 870 1
- Drake, A. J., Graham, M. J., Djorgovski, S. G., et al. 2014, ApJS, 213, 9 1, 2
- Eastman, J., Siverd, R., & Gaudi, B. S. 2010, PASP, 122, 935 4
- Eggleton, P. 2006, Evolutionary Processes in Binary and Multiple Stars 1
- Eggleton, P. P. 1983, ApJ, 268, 368 9
- Eker, Z., Demircan, O., Bilir, S., & Karataş, Y. 2006, MNRAS, 373, 1483 13

- Gaia Collaboration. 2022, *VizieR Online Data Catalog*, I/355 11, 12
- Gajdoš, P., & Parimucha, Š. 2019, *Open European Journal on Variable Stars*, 197, 71 5, 14
- Ginsburg, A., Sipőcz, B. M., Brasseur, C. E., et al. 2019, *AJ*, 157, 98 14
- Guinan, E. F., & Bradstreet, D. H. 1988, in *NATO Advanced Study Institute (ASI) Series C, Vol. 241, Formation and Evolution of Low Mass Stars*, ed. A. K. Dupree & M. T. V. T. Lago, 345 12
- Harris, C. R., Millman, K. J., van der Walt, S. J., et al. 2020, *Nature*, 585, 357 14
- Hoffman, D. I., Harrison, T. E., McNamara, B. J., et al. 2006, *AJ*, 132, 2260 1
- Hu, K., Yu, Y.-X., Zhang, J.-F., & Xiang, F.-Y. 2020, *AJ*, 160, 62 1
- Huang, L. C., Ip, W. H., Lin, C. L., et al. 2020, *ApJ*, 892, 58 1
- Hunter, J. D. 2007, *Computing in Science & Engineering*, 9, 90 14
- Hurley, J. R., Tout, C. A., & Pols, O. R. 2002, *MNRAS*, 329, 897 13
- Jayasinghe, T., Kochanek, C. S., Stanek, K. Z., et al. 2018, *MNRAS*, 477, 3145 1
- Jayasinghe, T., Stanek, K. Z., Kochanek, C. S., et al. 2019, *MNRAS*, 486, 1907 1, 2
- Jayasinghe, T., Stanek, K. Z., Kochanek, C. S., et al. 2020, *MNRAS*, 493, 4045 1
- Kjurkchieva, D., Stateva, I., Popov, V. A., & Marchev, D. 2019, *AJ*, 157, 73 1
- Kwee, K. K., & van Woerden, H. 1956, *Bull. Astron. Inst. Netherlands*, 12, 327 3
- Lanza, A. F., Rodono, M., & Rosner, R. 1998, *MNRAS*, 296, 893 1
- Li, K., Xia, Q.-Q., Kim, C.-H., et al. 2021, *AJ*, 162, 13 2, 12, 13
- Li, L., & Zhang, F. 2006, *MNRAS*, 369, 2001 12
- Lightkurve Collaboration, Cardoso, J. V. d. M., Hedges, C., et al. 2018, *Lightkurve: Kepler and TESS time series analysis in Python*, *Astrophysics Source Code Library*, ascl:1812.013 14
- Lu, L.-N., Liu, J.-Z., Jiang, D.-K., & Wang, Y.-H. 2020, *Research in Astronomy and Astrophysics*, 20, 196 9
- Lucy, L. B. 1967, *ZAp*, 65, 89 6, 11
- Lucy, L. B., & Wilson, R. E. 1979, *ApJ*, 231, 502 11
- Ma, S., Li, K., Li, Q. C., & Gao, H. Y. 2018, *New Astron.*, 59, 1 1
- Maíz Apellániz, J. 2006, *AJ*, 131, 1184 10
- Malkov, O. Y., Oblak, E., Snegireva, E. A., & Torra, J. 2006, *A&A*, 446, 785 1
- Marigo, P., Girardi, L., Bressan, A., et al. 2008, *A&A*, 482, 883 10
- Montes, D., de Castro, E., Fernandez-Figueroa, M. J., & Cornide, M. 1995, *A&AS*, 114, 287 6
- O'Donnell, J. E. 1994, *ApJ*, 422, 158 10
- Pawlak, M., Pejcha, O., Jakubčík, P., et al. 2019, *MNRAS*, 487, 5932 1
- Pecaut, M. J., & Mamajek, E. E. 2013, *ApJS*, 208, 9 11
- Ricker, G. R., Winn, J. N., Vanderspek, R., et al. 2014, in *Society of Photo-Optical Instrumentation Engineers (SPIE) Conference Series, Vol. 9143, Space Telescopes and Instrumentation 2014: Optical, Infrared, and Millimeter Wave*, ed. J. Oschmann, Jacobus M., M. Clampin, G. G. Fazio, & H. A. MacEwen, 914320 1
- Ricker, G. R., Winn, J. N., Vanderspek, R., et al. 2015, *Journal of Astronomical Telescopes, Instruments, and Systems*, 1, 014003 1
- Ruciński, S. M. 1969, *Acta Astronomica*, 19, 245 6
- Schlafly, E. F., & Finkbeiner, D. P. 2011, *ApJ*, 737, 103 11
- Soderblom, D. R., Stauffer, J. R., Hudon, J. D., & Jones, B. F. 1993, *ApJS*, 85, 315 5
- Strassmeier, K., Washuettl, A., Granzer, T., Scheck, M., & Weber, M. 2000, *A&AS*, 142, 275 6
- Street, R. A., Pollaco, D. L., Fitzsimmons, A., et al. 2003, in *Astronomical Society of the Pacific Conference Series, Vol. 294, Scientific Frontiers in Research on Extrasolar Planets*, ed. D. Deming & S. Seager, 405 1
- Tang, J., Bressan, A., Rosenfield, P., et al. 2014, *MNRAS*, 445, 4287 10
- Tody, D. 1986, in *Society of Photo-Optical Instrumentation Engineers (SPIE) Conference Series, Vol. 627, Instrumentation in astronomy VI*, ed. D. L. Crawford, 733 14
- Tody, D. 1993, in *Astronomical Society of the Pacific Conference Series, Vol. 52, Astronomical Data Analysis Software and Systems II*, ed. R. J. Hanisch, R. J. V. Brissenden, & J. Barnes, 173 14
- Torres, G. 2010, *AJ*, 140, 1158 11
- Tout, C. A., & Hall, D. S. 1991, *MNRAS*, 253, 9 11
- van Hamme, W. 1993, *AJ*, 106, 2096 6
- Wang, Y.-H., Liu, J.-Z., Lu, L.-N., & Lü, G.-L. 2019, *Research in Astronomy and Astrophysics*, 19, 108 9
- Whelan, D. G., Chojnowski, S. D., Labadie-Bartz, J., et al. 2021, *AJ*, 161, 67 1
- Wilson, R. E. 1979, *ApJ*, 234, 1054 6
- Wilson, R. E. 1990, *ApJ*, 356, 613 6
- Wilson, R. E. 2008, *ApJ*, 672, 575 6
- Wilson, R. E. 2012, *AJ*, 144, 73 6
- Wilson, R. E., & Devinney, E. J. 1971, *ApJ*, 166, 605 6
- Wilson, R. E., Van Hamme, W., & Terrell, D. 2010, *ApJ*, 723, 1469 6
- Yang, F., Long, R. J., Shan, S.-S., et al. 2020, *ApJS*, 249, 31 2, 4, 5

- Yang, Y.-G., & Qian, S.-B. 2015, *AJ*, 150, 69 12
- Yıldız, M. 2014, *MNRAS*, 437, 185 10
- Yıldız, M., & Doğan, T. 2013, *MNRAS*, 430, 2029 1
- Zhang, J., Qian, S.-B., Han, Z.-T., & Wu, Y. 2017, *MNRAS*, 466, 1118 8, 9
- Zhang, J., Bi, S., Li, Y., et al. 2020, *ApJS*, 247, 9 5